Eur. J. Mineral.
2004, **16**, 567–576

Kinetics of deuteration in pyrope

MARC BLANCHARD* and JANNICK INGRIN

Laboratoire Mécanismes de Transfert en Géologie, U. M. R. 5563, Equipe de Minéralogie, CNRS – Université Paul Sabatier, 39 allées Jules Guesde, F-31000 Toulouse, France
* Corresponding author, e-mail: blanchar@cict.fr

Abstract: Hydrogen-deuterium exchange experiments were performed at temperatures between 973 and 1223 K on a Dora Maira pyrope and on two pyrope samples from mantle xenoliths. The Fourier transform infrared (FTIR) spectra of hydrogen in the natural Dora Maira and xenolith pyropes are different, with several OH bands between 3600 and 3650 cm^{-1} and between 3510 and 3575 cm^{-1}, respectively. The self-diffusion of deuterium in Dora Maira pyrope is given by $D = D_0 \exp [-140 \pm 38\ kJmol^{-1}/RT]$ with $\log D_0\ (m^2/s) = -5.8 \pm 1.9$. This activation energy for diffusion is identical to those measured in diopside and olivine, but the pre-exponential term D_0 is one to two orders of magnitude smaller. This suggests that the mechanism of hydrogen self-diffusion in the pyrope structure is similar to that for other upper mantle mineral structures, such as olivine and pyroxene. In contrast to the Dora Maira pyrope, for the two pyrope crystals extracted from xenoliths, the total concentration of hydrous species is not preserved during H-D exchange experiments; dehydration occurs concurrently with deuteration. This renders the analysis of the kinetics of H-D exchange difficult. In the pyropes from mantle xenoliths, the kinetics of dehydration under reducing conditions is close to that for hydrogen dehydrogenation from experiments performed in air by Wang *et al.* (1996). This suggests that hydrogen exchange in mantle pyropes may be independent of the oxygen fugacity.

Key-words: pyrope, hydrogen, water, upper mantle, diffusion.

1. Introduction

Incorporation of small amounts of hydrogen in nominally anhydrous minerals is an important part of the process of recycling water into the Earth's interior (Thompson, 1992; Bell & Rossman, 1992a; Ingrin & Skogby, 2000; Williams & Hemley, 2001). Kinetic data on hydrogen mobility in upper mantle minerals are essential to understand the dynamics of this cycle and the origin of hydrogen concentrations preserved in mantle xenoliths (Bell & Rossman, 1992b; Matsyuk *et al.*, 1998; Jamveit *et al.*, 2001; Peslier *et al.*, 2002). Several kinetic studies have been conducted on olivine and pyroxenes (Mackwell & Kohlstedt, 1990; Hercule & Ingrin, 1999; Carpenter Woods *et al.*, 2000; Stalder & Skogby, 2003; Demouchy & Mackwell, 2003). For garnet, very few data exist on hydrogen mobility despite the great variety of OH infrared signatures observed in this structure and the numerous studies published on the subject (Ackermann *et al.*, 1983; Aines & Rossman, 1984; Rossman *et al.*, 1989; Rossman & Aines, 1991; Geiger *et al.*, 1991; Khomenko *et al.*, 1994; Amthauer & Rossman, 1998; Withers *et al.*, 1998; Geiger *et al.*, 2000). Wang *et al.* (1996) performed dehydrogenation experiments on natural pyrope megacrysts in air; these data on mantle-derived garnets do not elucidate the mechanism of hydrogen exchange operating within the garnet structure, nor the influence of the nature of hydrogen defects on kinetics. In clinopyroxenes, the rate laws for hydrogen-deuterium (H-D) exchange and H extraction in air have comparable activation energy (around 140 kJ/mol); the kinetics of H-D exchange is of the same order or faster than the extraction in air depending on the iron content (Hercule & Ingrin, 1999). No kinetic data on the H-D exchange are available for garnets. The activation energy measured by Wang *et al.* (1996) for H extraction in pyrope is close to 250 kJ/mol.

We report in this paper kinetic results for H-D exchange in two kinds of pyrope: a metamorphic pyrope of nearly end-member composition from the Dora Maira massif (western Alps) and two mantle-derived xenolith pyropes extracted from a Russian and a Brazilian kimberlite pipe.

2. Experimental techniques

2.1. Starting materials

Dora Maira pyrope

The pyrope samples of metamorphic origin used for this study were prepared from a large pale pink single crystal of about 8.5 mm in diameter collected by C. Chopin in the Dora Maira massif. They belong to the famous UHPM rocks from the outcrop described in Chopin (1984). The crystal is

DOI: 10.1127/0935-1221/2004/0016-0567
0935-1221/04/0016-0567 $ 4.50

Table 1. Structural formulae calculated on the base of 12 O and end-member cation proportions for the three pyrope single crystals.

Site	Cation	Dora Maira,core (9)	Dora Maira, edge (3)	3BT (2)	MGAK-2 (2)
X	Mg	2.431 ± 0.005	2.626 ± 0.026	2.091 ± 0.003	2.199 ± 0.003
	Fe^{2+}	0.445 ± 0.023	0.269 ± 0.013	0.551 ± 0.001	0.413 ± 0.031
	Ca	0.107 ± 0.005	0.079 ± 0.001	0.378 ± 0.002	0.407 ± 0.008
	Mn	0.004 ± 0.003	0.001 ± 0.001	0.021 ± 0.001	0.016 ± 0.002
		2.987	2.975	3.041	3.035
Y	Al^{VI}	1.985 ± 0.011	1.989 ± 0.009	1.682 ± 0.008	1.644 ± 0.020
	Fe^{3+}	0.013 ± 0.019		0.118 ± 0.026	0.075 ± 0.054
	Cr	0.001 ± 0.001	0.001 ± 0.001	0.087 ± 0.008	0.203 ± 0.001
	Ti		0.001 ± 0.001	0.071 ± 0.001	0.034 ± 0.001
		1.999	1.991	1.958	1.956
Z	Si	3.004 ± 0.016	3.019 ± 0.014	2.972 ± 0.008	3.002 ± 0.023
	Al^{IV}	0.005 ± 0.007		0.028 ± 0.008	0.007 ± 0.010
		3.009	3.019	3.000	3.009
end-members					
Pyrope		81.4 %	88.3 %	68.7 %	71.6 %
Almandine		14.9 %	9.0 %	18.1 %	13.5 %
Grossular		2.9 %	2.6 %	2.0 %	0.4 %
Andradite		0.7 %	0.0 %	6.0 %	3.8 %
Spessartine		0.1 %	0.0 %	0.8 %	0.5 %
Uvarovite		0.0 %	0.1 %	4.4 %	10.3 %

Note: The number in parentheses indicates the analysis number done on each sample. Uncertainties correspond to standard deviations. The Fe^{3+}/Fe_{tot} ratio was calculated to equilibrate structural formulae but may not reflect the real value.

of the same origin as the pink samples used for the FTIR study by Rossman *et al.* (1989). The core of the crystal has a homogeneous composition $Py_{81}Al_{15}Gr_3$, but the Mg content increases in the outermost 2 mm toward the sample edge to reach a composition close to $Py_{88}Al_9Gr_3$ (Table 1). Five thin slices, from 2.5 to 8.5 millimetres wide and 392 to 520 microns thick were cut and carefully polished with alumina powder to 0.3 microns (Table 2).

The Dora Maira crystal contains a small number of chlorite inclusions (few microns to tens of microns), mainly distributed along planar healed cracks. Fig. 1 shows a high spatial resolution FTIR analysis performed on a single inclusion at the synchrotron facility at LURE in Orsay (Dumas *et al.*, 2000). The nature of the inclusions was also confirmed by transmission electron microscopy (Ingrin, unpublished data). The high intensity of the OH absorption, composed of a band at 3677 cm^{-1} and a doublet at 3570 and 3545 cm^{-1}, are typical, respectively, of OH in the trioctahedral 2:1 layer and an OH stretching mode of the interlayer hydroxides in chlorite (Farmer, 1974). Only thin slices free of inclusions were selected for the kinetic study.

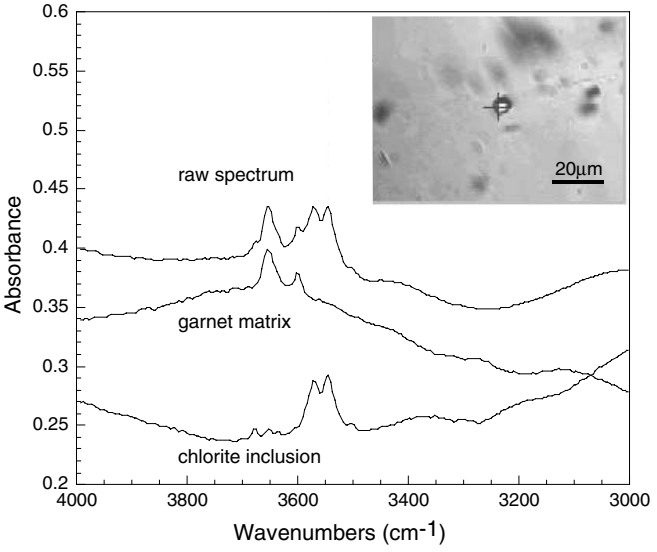

Fig. 1. High spatial resolution FTIR analysis performed on a single inclusion in Dora Maira pyrope at the synchrotron facility at LURE with a spot of 5 µm size. The OH infrared signature of the inclusion was obtained after removing the contribution of the garnet matrix. Sample thickness 392 µm.

Pyropes from mantle xenoliths

Two pyrope single crystals from kimberlite xenoliths were used for this study. Both samples were provided by S. S. Matsyuk: sample 3BT comes from the Mir pipe in the Malo-Botuobisnkoye field (Yakutia, Russia) and sample MGAK-2 is from the Akkuri pipe (Brazil). The two crystals are chemically homogeneous with compositions close to $Py_{69}Al_{18}And_6Uv_5Gr_2$ and $Py_{72}Al_{14}And_4Uv_{10}$, respectively (Table 1). Due to the small size of each crystal (around one mm wide in their lowest thickness), only one slice was cut per crystal (Table 2). Both slices were polished with alumina powder to 0.3 microns.

2.2. Annealing procedure

Heat treatments were carried out at ambient pressure in a horizontal furnace in which the sample was isolated from

Table 2. Experimental data for H-D and D-H exchange.

t (h)	t cor. (h)	A_H(cm^{-1})	ΔA_H(cm^{-1})	A_D(cm^{-1})	ΔA_D(cm^{-1})
Dora 2; 973 K; 2L = 0.500 mm; size = 8.5×4.5 mm^2					
H-D exchange					
0.00	0.00	1.15	0.05	0.01	0.01
2.00	2.29	1.28	0.05	0.01	0.01
6.00	6.58	1.08	0.05	0.07	0.03
12.00	12.86	0.98	0.05	0.11	0.05
24.00	25.15	0.96	0.05	0.15	0.05
40.00	41.86	0.81	0.05	0.20	0.05
72.00	74.15	0.58	0.05	0.33	0.05
136.00	138.44	0.31	0.05	0.51	0.04
268.00	270.72	0.05	0.05	0.75	0.03
406.73	409.74	0.01	0.05	0.77	0.03
606.73	610.03	0.00	0.05	0.78	0.03
Dora 9; 1023 K; 2L = 0.512 mm; size = 2.5×2.5 mm^2					
H-D exchange					
0.00	0.00	2.52	0.10	0.03	0.04
6.00	6.29	2.27	0.10	0.14	0.05
12.00	12.58	2.13	0.10	0.26	0.06
36.00	36.88	1.63	0.10	0.61	0.08
72.00	73.17	1.20	0.10	0.88	0.08
144.00	145.46	0.65	0.10	1.24	0.10
288.00	289.76	0.32	0.10	1.36	0.10
Dora 2; 1023 K; 2L = 0.500 mm; size = 8.5×4.5 mm^2					
D-H exchange					
0.00	0.00	0.00	0.05	0.78	0.03
6.00	6.29	0.26	0.05	0.50	0.03
12.00	12.58	0.41	0.05	0.43	0.03
24.00	24.88	0.71	0.05	0.28	0.03
48.00	49.17	0.95	0.05	0.11	0.03
96.00	97.46	1.07	0.05	0.02	0.03
Dora 3; 1073 K; 2L = 0.520 mm; size = 8.5×4.0 mm^2					
H-D exchange					
0.00	0.00	1.50	0.15	0.01	0.01
1.00	1.33	1.35	0.05	0.08	0.02
2.00	2.67	1.29	0.10	0.13	0.03
4.00	5.00	1.13	0.05	0.23	0.03
8.00	9.33	0.94	0.05	0.39	0.02
16.00	17.67	0.50	0.10	0.57	0.04
32.00	34.00	0.21	0.05	0.83	0.05
64.00	66.34	0.10	0.08	0.84	0.03
128.00	130.67	0.03	0.05	0.90	0.04
258.00	261.00	0.00	0.05	0.88	0.04
D-H exchange					
0.00	0.00	0.00	0.05	0.88	0.04
4.00	4.33	0.50	0.05	0.58	0.04
8.00	8.67	0.77	0.05	0.44	0.04
19.00	20.00	1.07	0.05	0.22	0.04
39.00	40.33	1.38	0.05	0.08	0.04
99.00	100.67	1.39	0.10	0.01	0.04

t (h)	t cor. (h)	A_H(cm^{-1})	ΔA_H(cm^{-1})	A_D(cm^{-1})	ΔA_D(cm^{-1})
Dora 4; 1123 K; 2L = 0.480 mm; size = 3.0×2.5 mm^2					
H-D exchange					
0.00	0.00	2.41	0.15	0.00	0.02
0.20	0.59	2.37	0.08	0.00	0.01
0.70	1.47	2.13	0.05	0.12	0.04
1.40	2.54	1.99	0.05	0.26	0.04
2.90	4.42	1.66	0.08	0.49	0.05
5.90	7.79	1.18	0.05	0.76	0.07
11.90	14.17	0.67	0.05	1.10	0.07
23.90	29.54	0.33	0.11	1.33	0.07
47.90	50.92	0.12	0.09	1.43	0.10
95.90	99.29	0.02	0.07	1.53	0.10
191.90	195.68	0.00	0.07	1.45	0.10
D-H exchange					
0.00	0.00	0.00	0.07	1.45	0.10
3.00	3.38	0.75	0.10	1.00	0.10
6.00	6.75	1.14	0.10	0.76	0.10
15.00	16.13	1.67	0.10	0.36	0.10
33.00	34.50	2.12	0.10	0.10	0.10
83.00	84.88	2.27	0.15	-0.01	0.10
Dora 5; 1223 K; 2L = 0.392 mm; size = 7.0×4.0 mm^2					
H-D exchange					
0.00	0.00	-	-	-	-
0.50	0.84	0.58	0.05	0.32	0.03
1.00	1.68	0.46	0.05	0.38	0.03
2.00	3.02	0.39	0.05	0.41	0.03
4.00	5.36	0.31	0.05	0.37	0.03
8.00	9.71	0.27	0.05	0.36	0.03
16.00	18.05	0.10	0.05	0.39	0.03
24.00	26.39	0.05	0.05	0.38	0.03
3BT; 973 K; 2L = 0.210 mm; size = 1.5×1.0 mm^2					
H-D exchange					
0.00	0.00	1.51	0.08	0.00	0.05
1.50	1.65	1.20	0.08	0.02	0.05
3.00	3.31	0.27	0.06	0.04	0.05
6.00	6.46	0.41	0.06	0.07	0.05
15.00	15.62	0.12	0.05	0.13	0.05
30.00	30.77	0.00	0.05	0.15	0.05
64.00	64.93	0.00	0.05	0.16	0.05
MGAK-2; 1123 K; 2L = 0.637 mm; size = 5.0×1.5 mm^2					
H-D exchange					
0.00	0.00	2.41	0.15	0.00	0.05
1.00	1.23	0.62	0.10	0.16	0.05
2.00	2.46	0.33	0.08	0.17	0.05
4.00	4.69	0.14	0.05	0.28	0.05
8.00	8.92	0.00	0.05	0.23	0.05
17.00	18.15	0.00	0.05	0.17	0.05
D-H exchange					
0.00	0.00	0.00	0.05	0.17	0.05
13.00	13.23	0.31	0.08	0.01	0.05

Note: t is the nominal time of heating, t cor., the time of heating after correction due to the durations of the heating ramps, A_H and A_D = the OH and OD integral absorbance, ΔA = the uncertainty on A, and 2L = the thickness of the sample. Sample Dora 5 has no initial spectrum.

the heating elements (lanthanium chromite) by an alumina tube of 18 mm internal diameter. Experimental temperatures ranged from 973 to 1223 K and were controlled by a Pt/Pt-Rh10% thermocouple located less than 5 mm from the sample. We estimate the uncertainty in temperature at the sample to be less than ± 5 K.

To perform the H-D and D-H exchanges, the reducing atmosphere around the samples was fixed, respectively, by a

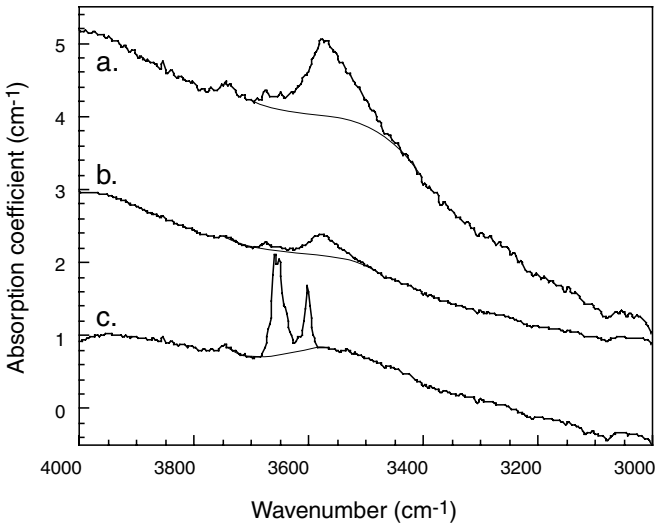

Fig. 2. Initial infrared absorption spectra of natural pyrope crystals: 3BT (a), MGAK-2 (b), and Dora Maira pyrope (c) (Dora 9). Thin lines correspond to the baseline used for the measurement of integral absorptions. Spectra are offset vertically for clarity.

90 % Ar + 10 % D_2 gas mixture flowing through deuterated water (99.8 % D_2O) and by a 90 % Ar + 10 % H_2 gas flowing through water. The alumina tube was flushed with the gas mixture for 30 minutes before the heating started. The ramp was programmed to reach the final temperature in 60 minutes.

2.3. Infrared analysis

The amount of hydroxyl in the slices was determined before and after each experiment by room-temperature transmission infrared spectroscopy using a Fourier transform spectrometer (Perkin-Elmer 1760), which was purged with dry air to minimize atmospheric contamination. Each spectrum was taken on the central part of the sample, as far as possible from the edges, through an aperture of 600 μm in diameter. The acquisition mode with an interleaved shuttle (a blank scan is automatically recorded every 4 scans) was chosen to correct in real time for the moisture remaining in the chamber atmosphere. An MCT detector cooled by liquid nitrogen was used to collect 512 scans at a resolution of 4 cm^{-1} between 4000 and 1500 cm^{-1} from a non-polarized infrared beam.

Fig. 2 shows the infrared spectra of the three starting materials used for this study. The 3BT and MGAK-2 spectra show the typical OH absorption bands of mantle garnets recovered from basalts or kimberlites (Bell *et al.*, 1995; Matsyuk *et al.*, 1998); the strongest band is located at 3575 cm^{-1} with a shoulder around 3510 cm^{-1} (a weak band is also visible around 3675 cm^{-1}). In the Dora Maira pyrope, the infrared spectrum is composed of four narrow OH absorption bands located at 3661; 3651; 3641 and 3602 cm^{-1} (Rossman *et al.*, 1989). The small bands observed at 3750 cm^{-1} are an artefact of the spectrometer and are not related to the sample. The structural OH content of xenolith samples can be deduced from FTIR measurements using the calibration of Bell *et al.* (1995). The 3BT and MGAK-2 garnets contain 512 ± 8 and 27 ± 5 ppm (wt) H_2O, respectively. In Dora Maira pyrope, the OH bands appear at different wavenumbers than in the xenoliths; we can use either the Bell *et al.* (1995) or Libowitzky & Rossman (1997) calibration to obtain estimates of the OH content. The concentration measured in the different slices varies from 19 to 36 or from 13 to 26 ppm (wt) H_2O, respectively, depending on the calibration used.

The OH and OD integral absorbances, A_H, A_D, were measured by subtracting a baseline fit, which was established by a polynomial interpolation from 6 points taken on both sides of windows 3684 – 3570 cm^{-1} / 2714 – 2632 cm^{-1} for Dora Maira, 3700 – 3422 cm^{-1} / 2730 – 2596 cm^{-1} for 3BT and 3714 – 3498 cm^{-1} / 2702 – 2578 cm^{-1} for MGAK-2. The quality of the fit was always visually checked to ensure that there was no systematic misfit (Fig. 2). The ranges of integration windows were chosen as narrow as possible and the shapes of the baselines were the same as the spectra of completely dehydrogenated samples. For the two mantle crystals, due to the low intensity of the OD bands, we proceeded by successive subtractions in order to measure the OD gain at each step of the annealing.

Uncertainties in the absorbance measurements were estimated from the reproducibility of the spectral analysis and the fluctuations of integral absorbance due to variations in the estimation of the baseline. According to Beer's law, we assume in the following that the ratio of hydrogen concentrations in the same sample is equal to the ratio of measured integral absorbance since the sample thickness is constant during the succession of runs.

2.4. Analytical solution

Because the thickness of the sample is small compared to its width, we assume that diffusion is essentially one dimensional and can be described by equations for an infinite plate with a homogeneous initial concentration. In this geometry, the solution of the Fick's second law (Carslaw & Jaeger, 1959) for a concentration C of OH or OD as a function of the location x in the sample and time of heating t, can be expressed as,

$$C(x,t) = \frac{4C_0}{\pi} \sum_{n=0}^{\infty} \frac{(-1)^n}{2n+1} \exp\left(\frac{-D\,t\,(2n+1)^2\,\pi^2}{4L^2}\right) \cos\frac{(2n+1)\,\pi\,x}{2L} \quad (1)$$

with the following boundary conditions: C = 0 for x = –L and x = +L for any t; C = C_0 for –L < x < +L at t = 0; C = C(x,t) for –L < x < +L at t > 0; where D is the diffusion coefficient of the mobile species, and L the half-thickness of the sample. The IR analysis gives only the average defect concentration, integrated over the sample thickness. The integration of (1) from –L to +L gives the average concentration:

$$\frac{C_{av}(t)}{C_0} = \frac{8}{\pi^2} \sum_{n=0}^{\infty} \frac{1}{(2n+1)^2} \exp\left(\frac{-D\,t\,(2n+1)^2\,\pi^2}{4L^2}\right). \quad (2)$$

This solution is valid for the decreasing species during the H-D or D-H exchange experiments. To follow the evolution of the increasing species, the following equation must be

used (with C_s = the concentration at saturation at the conditions of the experiment):

$$\frac{C_{av}(t)}{Cs} = 1 - \text{equation (2)} \qquad (3)$$

The diffusion coefficient D has been extracted by fitting numerically equation (2) or (3) to the diffusion data, where C_{av}/C_0 or C_{av}/C_s are obtained from the results of the infrared measurements, and t is given by the duration of the experiments. No variation of the diffusion coefficient with OH concentration has been assumed in this study. This assumption is justified by the dilute concentration of hydrogen in pyrope. Moreover, the correct fit of the theoretical equation to the data does not justify complicating further the diffusion equation.

As a finite time is required to reach the nominal temperature of the experiment or to quench the sample to room temperature, the sample may undergo some exchange during the temperature ramps. A time correction, following the same procedure as Ingrin *et al.* (1995) was applied. This correction decreases the diffusion coefficients calculated from the results of the experiments by less than 10%. It has a negligible effect on the resulting activation energy. We assume for the analysis of results that hydrogen diffusion in cubic pyrope garnet is isotropic.

3. Results

3.1. Dora Maira pyrope

Pyrope slices were annealed in a deuterated gas mixture. The two main OH absorption bands are progressively replaced by OD bands at 2694 cm^{-1} and 2658 cm^{-1} (Fig. 3). The observed spectral wavenumber shift (ν_{OH}/ν_{OD}) is equal to 1.355 ± 0.001. This value is comparable to the ν_{OH}/ν_{OD} ratio measured in diopside (Hercule & Ingrin, 1999), and is in general agreement with data obtained from weak hydrogen bonds (Mikenda, 1986).

Except for the experiment at 1223 K (Fig. 3), no loss of hydrous component was observed during H-D exchange experiments. The value of the integral absorbance of the band related to deuterium at saturation (A_{Ds}), relative to that of H (A_{Hs}), is equal to the ratio of the molar absorption coefficients of OH versus OD, $\varepsilon_H/\varepsilon_D$, according to Beer's law

$$\frac{A_{Hs}}{A_{Ds}} = \frac{\varepsilon_H \times \text{path length} \times C_{OH}}{\varepsilon_D \times \text{path length} \times C_{OD}} = \frac{\varepsilon_H}{\varepsilon_D}$$

The compilation of the $\varepsilon_H/\varepsilon_D$ obtained from the four Dora Maira slices, for which the saturation concentration of H and D are equal, gives an average value of 1.56 ± 0.19 (σ).

The integral absorbances of OH and OD obtained after each run are reported in Table 2. In order to check if the experiments are reversible, we performed the exchange in both directions in three different slices (Dora 2-4). These data were fit by equations (2) and (3) according to the species used, to determine the diffusion coefficients (Fig. 4). The error bars on D are estimated by the extreme values that still fit the data within the experimental uncertainty on A. The sample annealed at the highest temperature 1223 K (Dora 5) exhibited a partial loss of the hydrous components during the H-D exchange. The sum of the OH and OD integral absorbances (modulated by the ratio of molar absorption coefficients) decreases from 1.08 cm^{-1} to 0.64 cm^{-1} after more than 24 h annealing. However, only the OH bands around 3660–3640 cm^{-1} are affected by the hydrogen escape; the band at 3602 cm^{-1} remains unchanged. Such behaviour was observed earlier by Bell *et al.* (1995; see their figure 3). In our experiment, the diffusion coefficient of H-D exchange was obtained by fitting the OH and OD bands at 3602 and 2658 cm^{-1} alone (Fig. 4f).

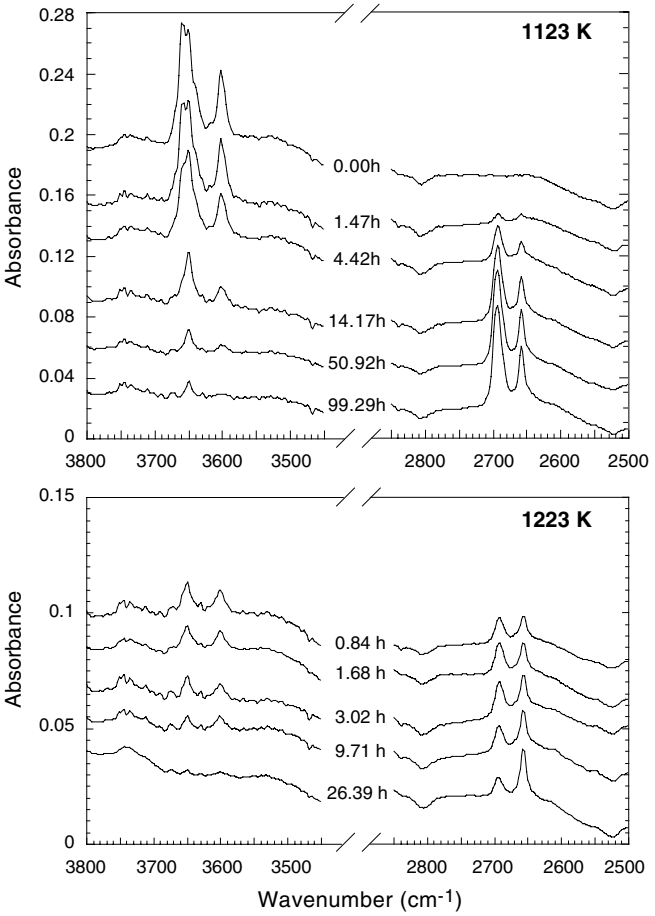

Fig. 3. Infrared spectra showing the progressive replacement of OH absorption bands by OD absorption bands with increasing time of heating in a deuterium environment. Samples Dora 4 and Dora 5 were heated at 1123 K and 1223K respectively, under reducing conditions. Spectra are offset vertically for clarity.

The resulting diffusion coefficients are summarized in an Arrhenius plot (Fig. 5). A least-squares fit, following the "least-squares cubic" method proposed by York (1966), leads to the diffusion law:

$$D = D_0 \exp\left[\frac{-(140 \pm 38)\ \text{kJ/mol}}{RT}\right]$$

$$\text{with } \log D_0 \text{ (in } m^2/s) = -5.8 \pm 1.9. \qquad (4)$$

The uncertainties were deduced from the least-squares fitting uncertainty which takes into account the uncertainties

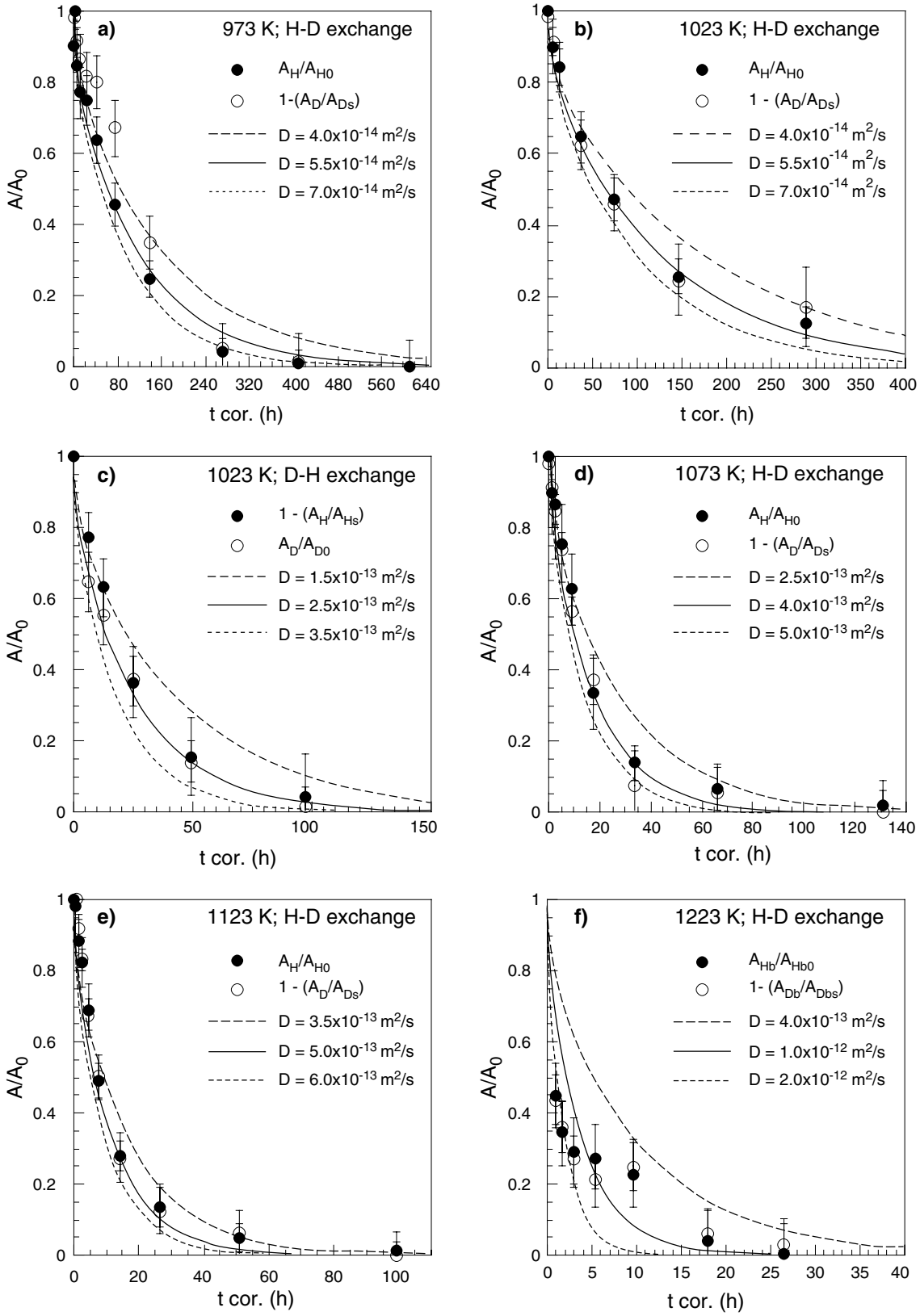

Fig. 4. Fit of deuteration data by Eq. (2) and (3) for different values of diffusion coefficient, D, in Dora Maira pyrope. Error bars on D were obtained from the range of D values that still fit the data (dashed lines). Only H-D exchanges are shown here except for 1023 K where the D-H exchange was conducted on a different sample than for H-D exchange. The evolution of OH bands is represented by solid circles and the OD bands by empty circles. Fig. 4b, the OD integral absorbance at saturation (A_{Ds}) is not known since the H-D exchange has not been completed, so its value was calculated from the ratio $\varepsilon_H/\varepsilon_D$.

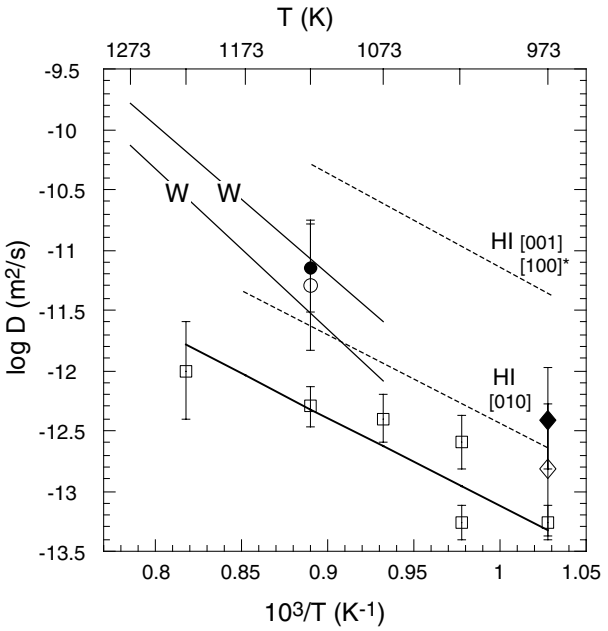

Fig. 5. Diffusivities for H-D exchange: in Dora Maira pyrope (empty squares fitted by the thick line); in pyropes from xenoliths (empty circle, MGAK-2; empty diamond, 3BT); and for H extraction in pyropes from xenoliths (solid circle, MGAK-2; solid diamond, 3BT). Results for hydrogen diffusivities in other mantle phases is also illustrated: W: H extraction in pyropes (Wang *et al.*, 1996); HI: H-D exchange in diopside in three crystallographic directions (Hercule & Ingrin, 1999).

in both D and 1/T. We will assume in the following that the above diffusion law represents the self-diffusion of hydrogen or deuterium in Dora Maira pyrope.

3.2. Pyropes from mantle xenoliths

Deuteration experiments performed on the slices of 3BT and MGAK-2 lead to faster kinetics than in the Dora Maira samples. The main OD band occurs at 2638 cm^{-1} (ν_{OH}/ν_{OD} = 1.355); the integral absorbances of OH and OD bands are reported in Table 2. For the two temperatures investigated, extraction of the hydrous components occurs while deuterium is replacing hydrogen. The extraction kinetics are quantified by plotting the sum of the OH and OD integral absorbances, modulated by the ratio of molar absorption coefficients (Fig. 6a, b). We used for this purpose the ratio of molar absorption coefficients ($\varepsilon_H/\varepsilon_D$) determined from the Dora Maira slices. A change of ($\varepsilon_H/\varepsilon_D$) within its uncertainty range (10–15 %) has almost no effect on the value of the diffusion coefficients obtained from Fig. 6a, b.

The diffusion coefficients for the xenolith pyropes are reported in the Arrhenius plot in Fig. 5; they are very close to the upper limit of the extraction kinetics found by Wang *et al.* (1996) and their extrapolation toward lower temperatures, even though in our experiments the oxygen fugacity is at least eighteen orders of magnitude lower than in air. For both samples, the concentration of hydrous species reached a constant value at the end of experiments equal to 10 to 20 % of the hydrogen concentration of the natural crystals (of the order of 3 to 10 ppm (wt) H_2O; Fig. 6a,b). This steady state behaviour is also confirmed by the result of the 13 h inverse exchange, D-H, performed on sample MGAK-2 (Table 2).

The H-D exchange kinetics can be bracketed by plotting: (1) the OH integral absorbances normalized to the initial value, leading to an overestimate of the diffusion coefficient due to the simultaneous extraction accelerating the apparent hydrogen decrease (Fig. 6c, d); or (2) the OD integral absorbances divided by the total content of deuterium and hydrogen (modulated by $\varepsilon_H/\varepsilon_D$) for each corresponding time of annealing (Fig. 6c, d). For these data, the fit by equation (3), gives an underestimated value of the H-D exchange kinetics. The error bars for these latter data are much larger due to the low deuterium content; this leads to mean values of 1.5 x 10^{-13} and 5.0 x 10^{-12} m^2/s, respectively at 973 and 1123 K. These two data points, reported in Fig. 5, fall in the same range as the hydrogen extraction in air (Wang *et al.*, 1996), and around half an order of magnitude above the H-D exchange law established for Dora Maira pyrope.

The study of the H-D exchange in the two mantle pyropes was greatly disrupted by the simultaneous occurrence of dehydrogenation. The kinetics of the dehydrogenation and the H-D exchange are so close that the uncertainty on the deuterium diffusion coefficients was too high to truly constrain the activation energy diffusion in these two pyropes.

4. Discussion

We assume in Eq. (2) and (3) that the diffusion occurs essentially along one crystallographic direction. The validity of this assumption has been tested by comparing the results of these equations with the results of a three-dimensional analysis of the diffusion in a rectangular parallelepiped of the same size as our slices (see Ingrin *et al.*, 1995). We observed almost no change in the results of the fits to the data.

4.1. Hydrogen-deuterium interdiffusion

Fig. 5 shows a comparison between the hydrogen diffusion laws in Dora Maira pyrope and diopside. In diopside, the reported diffusion laws correspond to H-D exchange experiments (Hercule & Ingrin, 1999) and so represent the hydrogen self-diffusion along the three crystallographic directions in this mineral phase. For Dora Maira pyrope, the kinetics of H-D exchange is identical for both groups of OH absorption bands, at least for experiments performed below 1223 K (Fig. 3) and represents almost the same activation energy as for diopside (145 kJ/mol). Kohlstedt & Mackwell (1998) obtained comparable activation energies (110 to 180 kJ/mol) for hydrogenation experiments performed on San Carlos olivine. These authors suggested that the rate of hydrogenation reaction in olivine is controlled by the self-diffusion of hydrogen (Kohlstedt & Mackwell, 1998). Thus, the mechanism of hydrogen mobility is expected to be the same for these three minerals.

In the mantle pyropes investigated in this study, the hydrogen self-diffusion has almost the same kinetics as that for

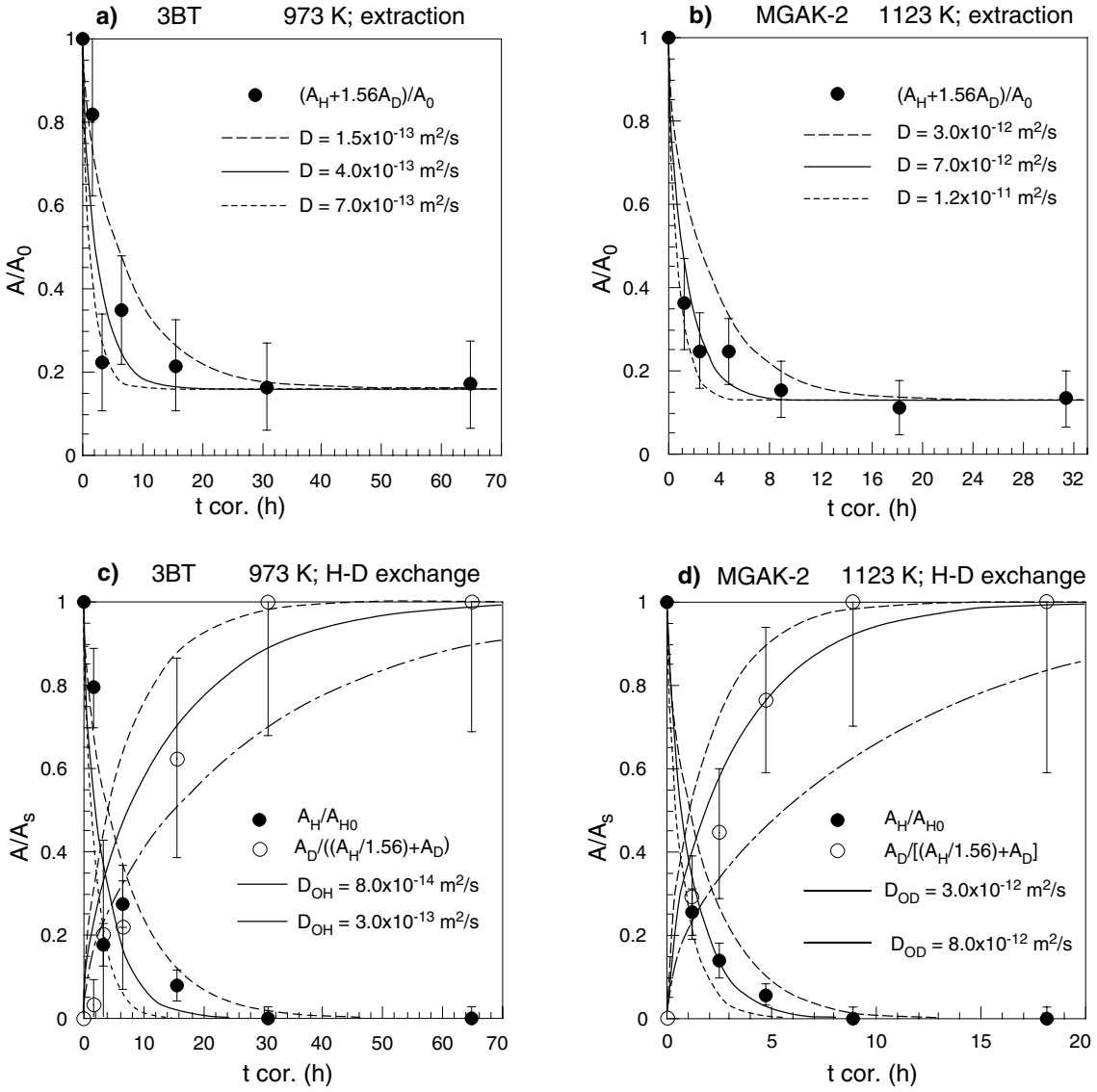

Fig. 6. Fit of extraction data of hydrous components (a, b) and of deuteration data (c, d) by Eq. (2) and (3) for different diffusion coefficients, D, in mantle pyropes. Diagrams on the left side correspond to sample 3BT, on the right side to sample MGAK-2. Error bars on D were deduced from the range of D values that still fit the data (dashed lines).

the slowest crystallographic directions of diopside (Fig. 5). The large uncertainty in the measurements due to the simultaneous dehydrogenation and the small sample sizes, render difficult any determination of the activation energy. However, an energy comparable to the one determined for Dora Maira pyrope (≈ 140 kJ/mol) is consistent with the data.

In the Dora Maira pyrope, hydrogen self-diffusion is five times slower than in the mantle pyropes or in diopside along the slowest direction. However, the difference between the diffusion coefficients of these two kinds of pyrope is small compared to the differences observed within a single mineral like diopside (Hercule & Ingrin, 1999). The main difference between the two types of pyropes is in the frequency position of their OH bands. The strong OH bands of the Dora Maira sample with the highest wavenumbers (75 to 90 cm^{-1} above those for the mantle pyropes) have the slowest diffusion rate.

4.2. Hydrogen extraction

The diffusion coefficients for hydrogen extraction in mantle pyropes deduced from the dehydrogenation occurring during the two H-D exchange experiments under reducing conditions ($6 \times 10^{-23} < pO_2 < 2 \times 10^{-19}$ atm) are comparable to the apparent bulk diffusion out coefficients (D^*_{out}) measured from extraction experiments performed in air (0.21 atm) by Wang *et al.* (1996) (Fig. 5; Wang's garnet compositions Py_{67} to Py_{72}). This result suggests that the extraction kinetics in mantle pyropes is not affected by the oxygen fugacity. The hydrogen diffusion in the mantle pyropes is at least as fast as in other major mantle phases (olivine, diopside). For the upper mantle (between 1000 and 1400°C), the coefficients of hydrogen exchange would lie between 4.0×10^{-10} and 3.5×10^{-8} m^2/s.

However, for metamorphic pyropes like the ones from Dora Maira, at least under reducing atmosphere, the kinetics

of hydrogen extraction is much slower than in xenolith pyropes because almost no loss of hydrogen and deuterium occurs during our H-D exchange experiments (except at 1223 K). The observation that some dehydrogenation occurs during the H-D exchange only at the highest temperature of 1223 K suggests that the activation energy for hydrogen extraction is probably higher than that for H-D exchange.

The spectral evolution of the Dora Maira sample annealed at 1223 K shows that the extraction only affects the triplets centred at 3650 cm^{-1} (OH) and 2694 cm^{-1} (OD). The other absorption bands at 3602 and 2658 cm^{-1} remain stable for the entire run duration. This contrasting behaviour confirms the presence of at least two distinct H defects. It is already known that several H defects and several mechanisms of hydrogen incorporation may coexist in pyrope (Lager *et al.*, 1989; Rossman *et al.*, 1989; Rossman & Aines, 1991; Geiger *et al.*, 1991).

5. Conclusion

In this work, we determined the law of H-D exchange in Dora Maira pyrope. Changes in the two principal OH absorption bands follow the same kinetics:

$$D = D_0 \exp\left[-\frac{(140 \pm 38)\ \text{kJ/mol}}{RT}\right],$$

with $\log D_0\ (m^2/s) = -5.8 \pm 1.9$

This activation energy is close to those for H-D exchange in diopside (Hercule & Ingrin, 1999) and hydrogen incorporation in olivine (Kohlstedt & Mackwell, 1998). These Dora Maira garnet diffusion coefficients are marginally lower than those measured in diopside and olivine. H-D exchange in pyrope xenoliths from the mantle is around five times faster than in Dora Maira pyrope.

The kinetics of hydrogen extraction in mantle pyropes, under reducing conditions, is identical to the kinetics measured by Wang *et al.* (1996) in air. This result suggests that hydrogen exchange in mantle pyropes is independent of oxygen fugacity. The hydrogen extraction-incorporation in pyrope is as fast as in other major upper-mantle phases. For the Dora Maira pyrope, no kinetics of hydrogen extraction were measured but we can predict from the result of H-D exchange that the kinetics is at least one to two orders of magnitude slower than in the mantle pyropes.

Acknowledgements: The Dora Maira pyrope and pyropes from mantle xenoliths were kindly provided by Christian Chopin and S.S. Matsyuk, respectively. We thank Philippe de Parseval for electron microprobe analyses and Paul Dumas for his help during FTIR analyses at LURE. We also acknowledge R.C. Liebermann for his valuable comments on an early version of the manuscript. Helpful comments by Roland Stalder, Eugen Libowitzky and an anonymous reviewer are gratefully acknowledged. This study was partially supported by the EU through the Human Potential Program HPRM-CT-2000-0056.

References

Ackermann, L., Cemic, L., Langer, K. (1983): Hydrogarnet substitution in pyrope: a possible location for "water" in the mantle. *Earth Planet. Sci. Lett.*, **62**, 208-214.

Aines, R.D. & Rossman, G.R. (1984): The hydrous component in garnets: pyralspites. *Am. Mineral.*, **69**, 1116-1126.

Amthauer, G. & Rossman, G.R. (1998): The hydrous component in andradite garnet. *Am. Mineral.*, **83**, 835-840.

Bell, D.R. & Rossman, G.R. (1992a): Water in Earth's mantle: The role of nominally anhydrous minerals. *Science*, **255**, 1391-1397.

–, – (1992b): The distribution of hydroxyl in garnets from the subcontinental mantle of southern Africa. *Contrib. Mineral. Petrol.*, **111**, 161-178.

Bell, D.R., Ihinger, P.D., Rossman, G.R. (1995): Quantitative analysis of trace OH in garnet and pyroxenes. *Am. Mineral.*, **80**, 465-474.

Carpenter Woods, S., Mackwell, S., Dyar, D. (2000): Hydrogen in diopside: Diffusion profiles. *Am. Mineral.*, **85**, 480-487.

Carslaw, H.S. & Jaeger, J.C. (1959): "Conduction of heat in solids". 2nd ed., Oxford, 510 p.

Chopin, C. (1984): Coesite and pure pyrope in high-grade blueschists of the Western Alps: a first record and some consequences. *Contrib. Mineral. Petrol.*, **86**, 107-118.

Demouchy, S. & Mackwell, S. (2003): water diffusion in synthetic iron-free forsterite. *Phys. Chem. Minerals,* **30**, 486-494.

Dumas, P., Carr, G.L., Williams, G.P. (2000): Enhancing the lateral resolution in infrared microspectrometry by using synchrotron radiation: application and perspectives. *Analusis,* **28**, 68-74.

Farmer, V.C. (1974): The layer silicates. *in* "The infrared spectra of minerals" V.C. Farmer, ed., Mineralogical Society, London, 331-365.

Geiger, C.A., Langer, K., Bell, D.R., Rossman, G.R., Winkler, B. (1991): The hydroxide component in synthetic pyrope. *Am. Mineral.*, **76**, 49-59.

Geiger, C.A., Stahl, A., Rossman, G.R. (2000): Single-crystal IR- and UV/VIS-spectroscopic measurements on transition-metal-bearing pyrope: the incorporation of hydroxyde in garnet. *Eur. J. Mineral.*, **12**, 259-271.

Hercule, S. & Ingrin, J. (1999): Hydrogen in diopside: Diffusion, kinetics of extraction-incorporation, and solubility. *Am. Mineral.*, **84**, 1577-1587.

Ingrin, J. & Skogby, H. (2000): Hydrogen in nominally anhydrous upper mantle minerals: concentration levels and implications. *Eur. J. Mineral.*, **12**, 543-570.

Ingrin, J., Hercule, S., Charton, T. (1995): Diffusion of hydrogen in diopside: Results of dehydration experiments. *J. Geophys. Res.*, **100**, 15489-15499.

Jamtveit, B., Brooker, R., Brooks, K., Larsen, L.M., Pedersen, T. (2001): The water content of olivines from the North Atlantic Volcanic Province. *Earth Planet. Sci. Lett.*, **186**, 401-415.

Khomenko, V.M., Langer, K., Beran, A., Koch-Müller, M., Fehr, T. (1994): Titanium substitution and OH-bearing defects in hydrothermally grown pyrope crystals. *Phys. Chem. Minerals,* **20**, 483-488.

Kohlstedt, D.L. & Mackwell, S.J. (1998): Diffusion of hydrogen and intrinsic point defects in olivine. *Z. Phys. Chem.*, **207**, 147-162.

Lager, G.A., Armbruster, T., Rotella, F.J., Rossman, G.R. (1989): OH substitution in garnets: X-ray and neutron diffraction, infrared, and geometric-modeling studies. *Am. Mineral.,* **74**, 840-851.

Libowitzky, E. & Rossman, G.R. (1997): An IR absorption calibration for water in minerals. *Am. Mineral.*, **82**, 1111-1115.

Mackwell, S.J. & Kohlstedt, D.L. (1990): Diffusion of hydrogen in olivine: implications for water in the mantle. *J. Geophys. Res.*, **95**, 5079-5088.

Matsyuk, S.S., Langer, K., Hösch, A. (1998): Hydroxyl defects in garnets from mantle xenoliths in kimberlites of the Siberian platform. *Contrib. Mineral. Petrol.*, **132**, 163-179.

Mikenda, W. (1986): Stretching frequency versus bond distance correlation of O–-D(H)…Y(Y = N, O, S, Se, Cl, Br, I) hydrogen bonds in solid hydrates. *J. Mol. Struct.*, **147**, 1-15.

Peslier, A.H., Luhr, J.F., Post, J. (2002): Low water contents in pyroxenes from spinel-peridotites of the oxidized, sub-arc mantle wedge. *Earth Planet. Sci. Lett.*, **201**, 69-86.

Rossman, G.R. & Aines, R.D. (1991): The hydrous components in garnets: Grossular-hydrogrossular. *Am. Mineral.*, **76**, 1153-1164.

Rossman, G.R., Beran, A., Langer, K. (1989): The hydrous component of pyrope from Dora Maira Massif, Western Alps. *Eur. J. Mineral.*, **1**, 151-154.

Stalder, R. & Skogby, H. (2003): Hydrogen diffusion in natural and synthetic orthopyroxene. *Phys. Chem. Minerals*, **30**, 12-19.

Thompson, A.B. (1992): Water in the Earth's upper mantle. *Nature*, **358**, 295-302.

Wang, L., Zhang, Y., Essene, E.J. (1996): Diffusion of the hydrous component in pyrope. *Am. Mineral.*, **81**, 706-718.

Williams, Q. & Hemley, R.J. (2001): Hydrogen in the deep Earth. *Ann. Rev. Earth Planet. Sci.*, **29**, 365-418.

Withers, A.C., Wood, B.J., Caroll, M.R. (1998): The OH content of pyrope at high pressure. *Chemical Geol.,* **147**, 161-171.

York, D. (1966): Least-squares fitting of a straight line. *Can. J. Phys.*, **44**, 1079-1086.

Received 22 July 2003
Modified version received 17 February 2004
Accepted 18 March 2004